„Inverted" hysteresis in bilayer Fe(II) spin crossover system

*Aleksandra Tołoczko, Marcin Kaźmierczak, Vladyslav Maliuzhenko, Miłosz Siczek, Marek Weselski, Robert Bronisz**

Faculty of Chemistry, University of Wrocław, F. Joliot-Curie 14, 50-383, Wrocław, Poland

Contents: page

Materials and methods

Acetonitrile (HPLC grade, J.T. Baker) was dried by distillation over the calcium hydride. Pyridine (Alfa Aesar) was dried over KOH and distilled. 1*H*-1,2,3-triazole (Chemical Point), iron(II) tetrafluoroborate hexahydrate (Merck), 2-hydroxy-1,3-dichloropropane (Aldrich), stearoyl chloride (Aldrich) were used as delivered. Syntheses of iron(II) complexes were carried out under a nitrogen atmosphere using the standard Schlenk technique.

Elemental analyses for carbon, hydrogen and nitrogen were carried out using Vario ELcube analyzer. IR spectra were recorded with a JASCO FT/IR 6700 spectrometer in the range 4000-400 cm^{-1} wavenumbers region as nujol mull. ^{1}H and ^{13}C NMR spectra were recorded on Bruker Avance III 500 MHz spectrometer at room temperature. Temperature dependent measurements of the magnetic susceptibility for **1** were carried out with a Quantum Design MPMS3 (sample 1) and Quantum Design MPMS-XL-5 (samples 2 and 3) magnetometers under 1 T applied magnetic field with different rates of change of temperature (experimental details are given in the manuscript). Data have been corrected for the signal of the empty holder and for diamagnetism of the samples. DSC measurements were carried out with Mettler Toledo DSC 3 at 2, 5, 10 and 20 K/min.

Single crystal X-ray data collection and structure determination.

Single crystals of **L1** were obtained from crystallization in acetonitrile. Single crystals of the complex **1** suitable for single crystal X-ray diffraction studies were obtained directly from syntheses of macroscopic samples. Crystals were covered with oil and placed on a glass capillar with a drop of silicon grease. During low-temperature measurements, an Oxford Cryosystem cooling device was used. Low temperatures were achieved with a stream of cold nitrogen gas. Temperature measurements were first taken in cooling mode (250 – 80 K), and then after reaching 80 K in heating mode (up to 293 K). Between each measurement, the temperature was changed at a rate of 1 K/min. Structural studies were performed with a κ-geometry, four-circle XtaLAB Synergy R DW (Rigaku) diffractometer with rotating anode source using Mo-Kα (λ = 0.71073 Å) radiation and Hybrid Pixel Array Detector 150° (Rigaku). CrysAlisPro software was used to control the measurement procedure, data reduction, determine and refine the lattice parameters. The crystal structures were solved by dual-space recycling with the *SHELXT-2018*[1] program. The refinements were carried out with the SHELXL-*2018/3*[2] program using the full-matrix least-squares method. Olex2[3] was used as a refinement and analysis GUI program. Non-hydrogen atoms were refined with anisotropic thermal parameters and hydrogen atoms were included from geometric considerations. In the final refinement stages a riding model was used for C–H bonds. During the refinement of the disordered fragments constraints on atomic displacement parameters (EADP instruction) and geometric restraints (SADI, SAME, RIGU instructions) were used if appropriate. Diamond[4] program was used to make the figures and the Platon[5] program was used for geometric analysis of the weak interactions. CCDC **2515369** for **L1** and **2515216** and **2515367-2515368** for **1** contain the supplementary crystallographic data for

this paper. These data can be obtained free of charge from The Cambridge Crystallographic Data Centre via www.ccdc.cam.ac.uk/data_request/cif.

Synthesis of 2-hydroxy-1,3-di(1*H*-1,2,3-triazol-1-yl)propane. In a 500 mL round-bottom flask, 30.4 g (0.440 mol) of 1*H*-1,2,3-triazole, 17.6 g (0.440 mol) of sodium hydroxide, and 200 mL of acetonitrile were placed. The mixture was concentrated to dryness on a rotary evaporator. To the resulting sodium salt of 1,2,3-triazole, 25.8 g (0.200 mol) of 1,3-dichloropropan-2-ol and 250 mL of acetonitrile were added. The reaction mixture was stirred under reflux for 7 days. The mixture was then separated by decantation, and the solid residue was extracted with boiling acetonitrile (100 mL) twice. The combined acetonitrile solutions were concentrated on a rotary evaporator. The product was purified by column chromatography (silica gel, eluent: $CH_2Cl_2/CH_3CH/CH_3OH$ 1/0.1/0.05 (v/v)). Yield 9.11 g (23%, white solid). Anal. calcd (%) for $C_7H_8N_6O$ (M_w = 192.18 g/mol): C, 43.8, N, 43.7; H, 4.2; found (%): C, 43.5; N 43.1; H, 4.3. ^{1}H NMR (500 MHz, CD_3CN), d: 8.02 (d, J = 1.0 Hz, 2H), 7.74 (d, J = 1.0 Hz, 2H), 4.63 (m, 2H), 4.44 (m, 3H) ppm. ^{13}C NMR (500 MHz, CD_3CN), d: 134.3, 127.2, 70.0, 54.3 ppm. FTIR spectrum is presented below.

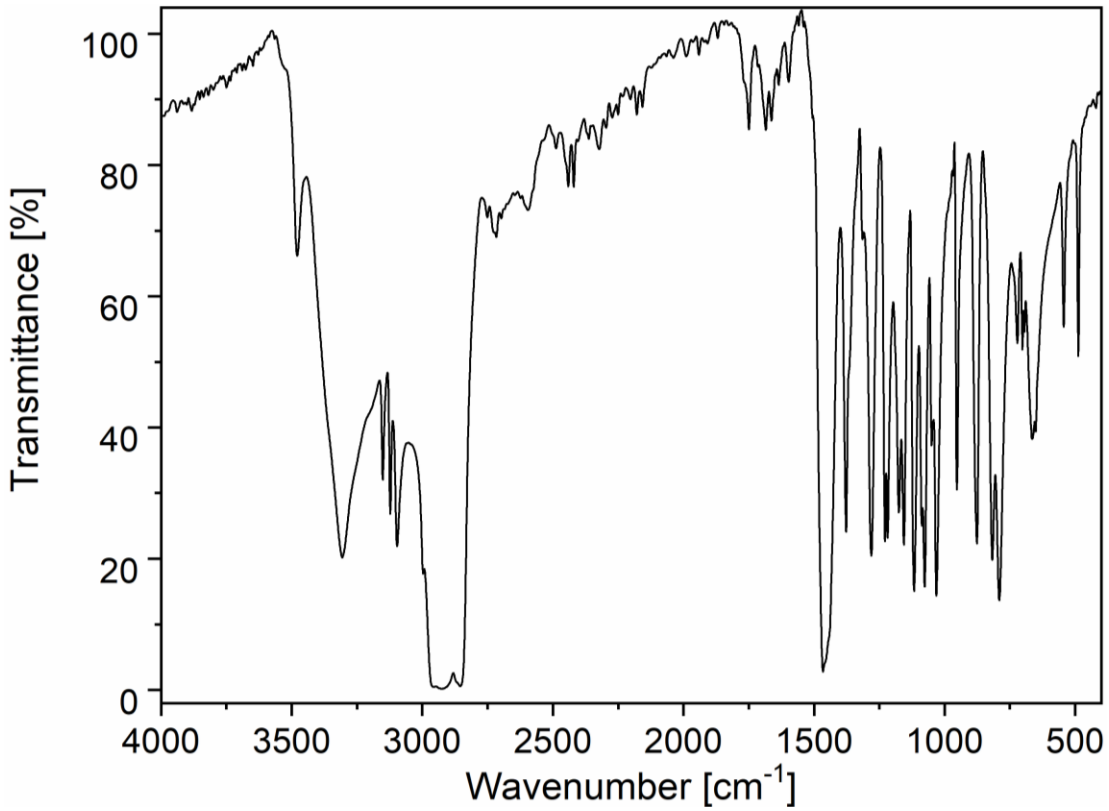

Synthesis of 1,3-di(1H-1,2,3-triazol-1-yl)propan-2-yl stearate. In a 100 mL round-bottom flask 0.560 g (2.80 mmol) of 1,3-di(1H-1,2,3-triazol-1-yl)propan-2-ol, 5 mL of pyridine, and 20 mL of dichloromethane were placed. To the vigorously stirred mixture 1.30 g (4.29 mmol) of the stearoyl chloride was added quickly, and the flask was sealed with a stopper. The reaction was carried out for 16 hours at room temperature. After completion, the resulting mixture was concentrated on a rotary evaporator. The crude product was separated by column chromatography (silica gel, eluent: $CH_2Cl_2/CH_3CN/CH_3OH$ 6-10/0.5-1/0.1-0.4 (v/v)). Yield: 0.930 g (72%, white solid). Anal. calcd (%) for $C_{25}N_6O_2H_{44}$ (M_w = 460.66 g/mol): C, 65.2; N, 18.2; H, 9.6; found (%): C, 65.1, N, 18.3, H, 9.8. ^{1}H NMR (500 MHz), δ (DMSO-d_6): 7.80 (d, J = 1.0 Hz, 2H), 7.65 (d, J = 1.0 Hz, 2H), 5.62 (m, 1H), 4.70 (dd, J = 15.0, 3.8 Hz, 2H), 4.54 (dd, J = 15.0, 7.4 Hz, 2H), 2.16 (t, J = 7.2 Hz, 2H), 1.39 (m, 2H), 1.27 (s, 24H), 0.88 (t, J = 6.8 Hz, 3H) ppm. ^{13}C NMR (500 MHz), δ (DMSO-d_6): 173.0, 134.4, 126.4, 70.8, 51.1, 34.4, 32.7, 30.4, 30.4, 30.3, 30.2, 30.0, 29.9, 29.6, 25.3, 23.4, 14.4 ppm. FTIR spectrum is presented below.

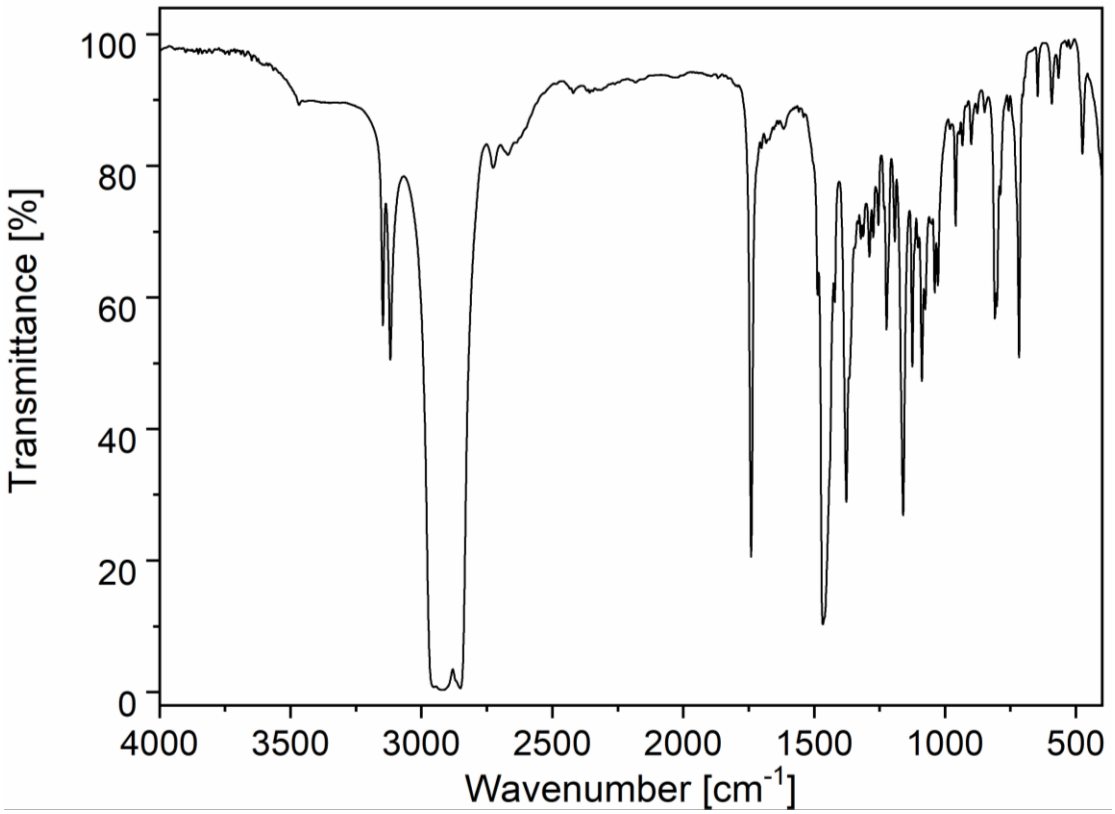

Scheme S1. Synthesis of **L1**.

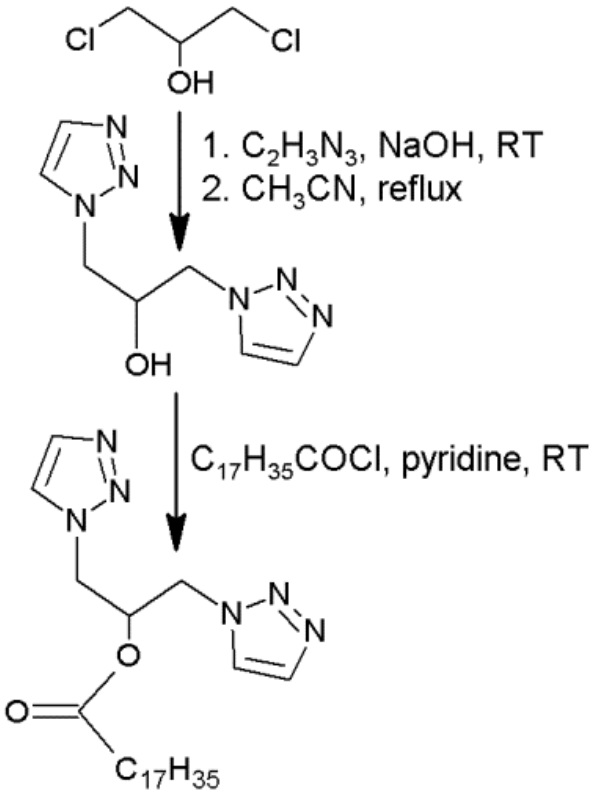

Synthesis of $[Fe(L1)_4](BF_4)_2 \cdot L1 \cdot 2CH_3CN \cdot 0.23H_2O$. 1,3-di(1*H*-1,2,3-triazol-1-yl)propan-2-yl stearate (0.100 mmol, 46.0 mg) was dissolved in 9 mL of dry acetonitrile. Subsequently, solution of $Fe(BF_4)_2 \cdot 6H_2O$ (0.0330 mmol, 11.0 mg) in 1 mL of acetonitrile was added. After mixing the reagents, the vessel was purged with nitrogen, sealed, and left at room temperature. After two days, the solution was concentrated while avoiding the appearance of any solid residue. After a month, the first microcrystals appear. The amount of product increased systematically over the following months. When the increase in the amount of product stopped, the crystalline sample was separated. Yield: 25.7 mg (15%, white solid). Anal. calcd (%) for $C_{129}H_{226.46}N_{32}B_2F_8O_{10.23}Fe$ (M_w = 2619.02 g/mol): C, 59.2%, N, 17.1%; H, 8.7%; found (%): C, 58.8%; N, 17.5%; H, 9.0%. FTIR spectrum is presented below.

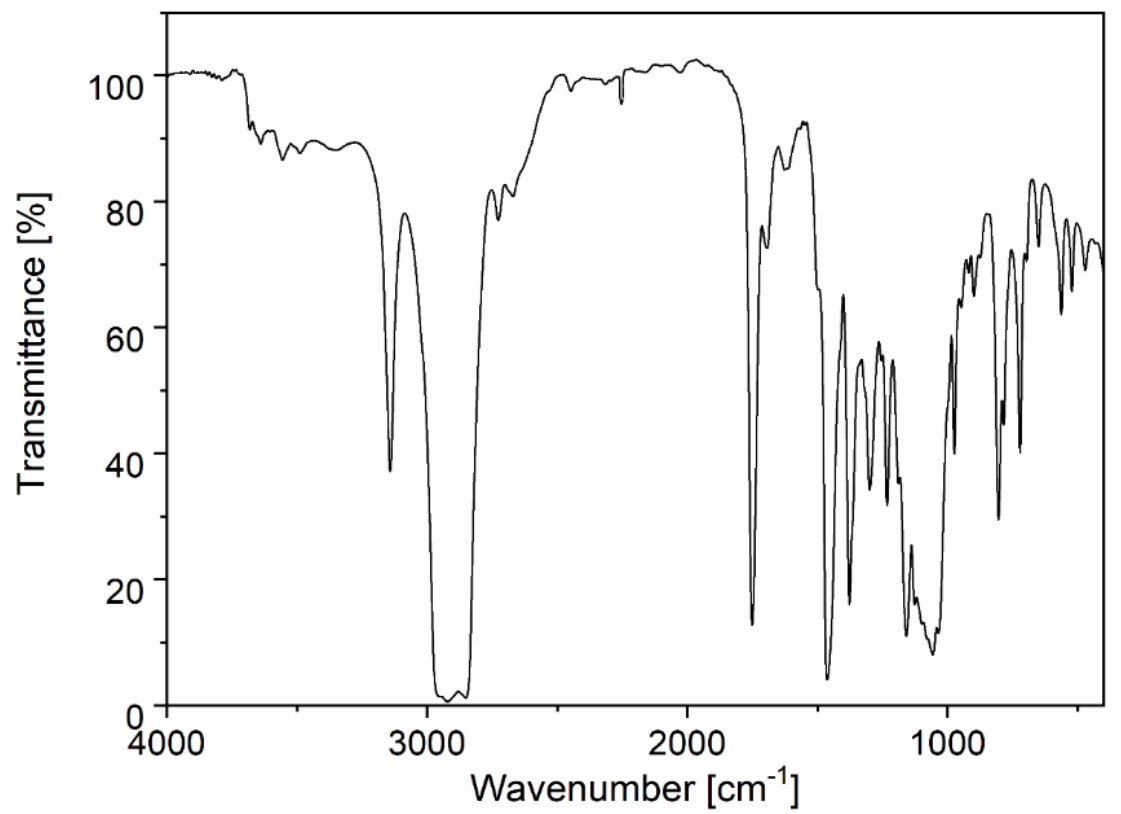
Transmittance [%]
100
80
60
40
20
0
4000
3000
2000
1000
Wavenumber [cm-1]

Table S1. Crystallographic data for crystal structure of **L1**.

CCDC number	**2515369**
Empirical formula	$C_{25}H_{44}N_6O_2$
Formula weight	460.66
Temperature/K	100
Crystal system	triclinic
Space group	*P-1*
***a*/Å**	5.376(2)
***b*/Å**	8.035(3)
***c*/Å**	31.164(8)
α/°	85.73(3)
β/°	88.55(3)
γ/°	74.99(4)
Volume/Å^3	1296.7(8)
Z	2
ρ_{calc}g/cm^3	1.180
μ/mm^{-1}	0.605
F(000)	504.0
Crystal size/mm^3	0.058 × 0.034 × 0.024
Radiation	Cu Kα (λ = 1.54184)
2Θ range for data collection/°	5.688 to 148.246
Index ranges	$-5 \le h \le 6$, $-9 \le k \le 9$, $-34 \le l \le 38$
Reflections collected	20255
Independent reflections	5039 [R_{int} = 0.0528, R_{sigma} = 0.0545]
Data/restraints/parameters	5039/0/299
Goodness-of-fit on F^2	1.147
Final R indexes [I>=2σ (I)]	R_1 = 0.0759, wR_2 = 0.1703
Final R indexes [all data]	R_1 = 0.1018, wR_2 = 0.1826
Largest diff. peak/hole / e Å^{-3}	0.28/-0.34

Crystal structure of L1. Single crystal of **L1** was grown from acetonitrile. **L1** crystallizes in triclinic *P-1* space group. The independent part of elementary unit consists of one ligand molecule. Alkyl chain adopts extended conformation. Molecules form layers within *ac* plane. The presence of long alkyl chains, arranged parallel to each other, exerts a profound influence on the relative position of neighboring molecules. As a result, a bilayer arrangement is formed, stabilized in the polar region by very weak contacts between the bisazole moieties (Fig. S1, Table S3).

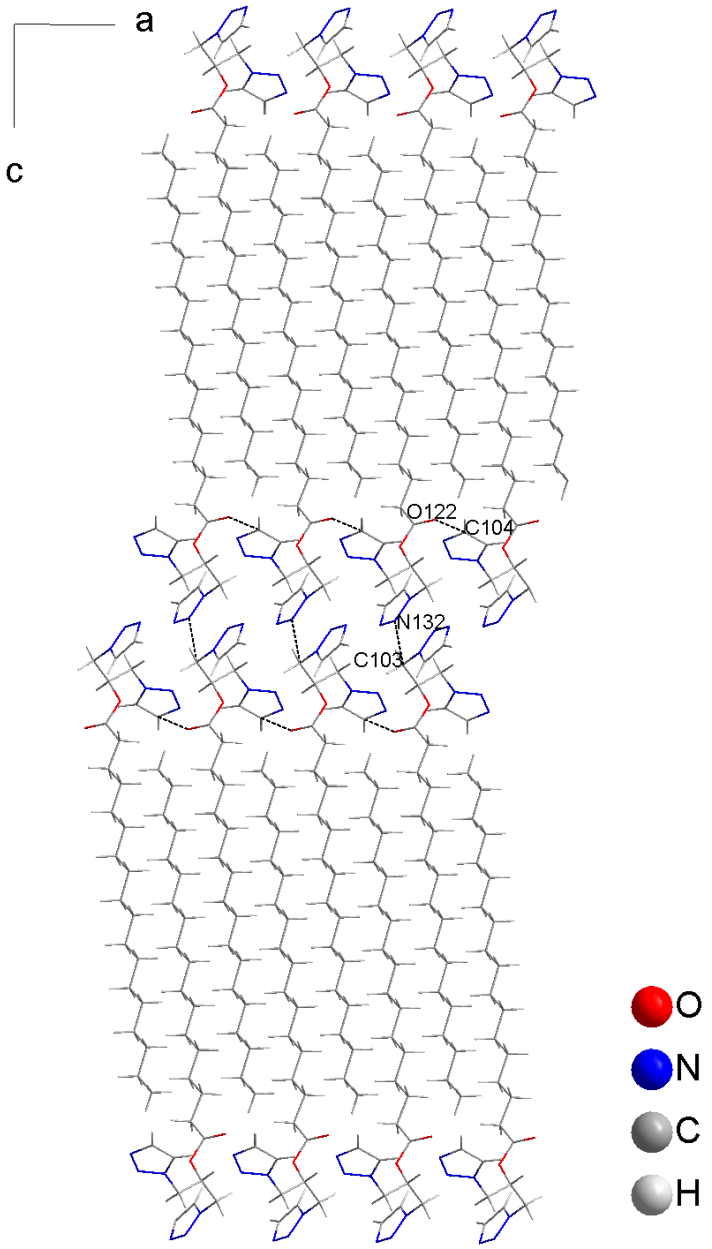

Figure S1. Crystal packing showing bilayer arrangement of **L1** molecules. Dotted lines indicate presence of intermolecular contacts within polar area.

Table S2. Crystallographic data for crystal structures of **1** at 293 K, 250 K and 80 K.

CCDC number	**2515368**	**2515367**	**2515216**
Empirical formula	**$[Fe_2(L1)_8](BF_4)_4 \cdot 2L1 \cdot 4CH_3CN \cdot 0.46H_2O$**		
Summary formula	$C_{258}H_{452.92}B_4F_{16}Fe_2N_{64}O_{20.46}$		
Formula weight	5238.04		
Temperature/K	**293**	**250**	**80**
Spin state	**HS**	**HS**	**LS**
Crystal system	triclinic		
Space group	*P-1*		
***a*/Å**	13.046(4)	13.001(4)	12.845(3)
***b*/Å**	18.844(7)	18.757(5)	18.464(3)
***c*/Å**	33.352(12)	33.217(8)	32.995(6)
α/°	78.27(3)	77.55(2)	75.73(2)
β/°	86.54(3)	85.89(2)	86.67(2)
γ/°	72.34(3)	72.53(2)	72.36(2)
Volume/Å^3	7650(5)	7545(4)	7226(3)
Z	1		
ρ_{calc}g/cm^3	1.137	1.153	1.204
μ/mm^{-1}	0.170	0.172	0.180
F(000)	2829.0		
Crystal size/mm^3	0.59 × 0.39 × 0.23		
Radiation	MoKα (λ = 0.71073)		
2Θ range for data collection/°	3.998 to 57.4		
Index ranges	-17 ≤ h ≤ 17 -25 ≤ k ≤ 25 -45 ≤ l ≤ 45	-17 ≤ h ≤ 17 -25 ≤ k ≤ 25 -44 ≤ l ≤ 44	-17 ≤ h ≤ 17 -24 ≤ k ≤ 24 -43 ≤ l ≤ 44
Reflections collected	220083	191638	180784
Independent reflections	39475 [R_{int} = 0.0495, R_{sigma} = 0.0399]	38902 [R_{int} = 0.0423, R_{sigma} = 0.0369]	37262 [R_{int} = 0.0489, R_{sigma} = 0.0413]
Data/restraints/parameters	39475/210/1858	38902/210/1864	37262/257/2186
Goodness-of-fit on F^2	1.030	1.054	1.158
Final R indexes [I>=2σ (I)]	R_1 = 0.0740, wR_2 = 0.1927	R_1 = 0.0685, wR_2 = 0.1855	R_1 = 0.0772, wR_2 = 0.1632
Final R indexes [all data]	R_1 = 0.1181, wR_2 = 0.2155	R_1 = 0.0980, wR_2 = 0.2007	R_1 = 0.0925, wR_2 = 0.1687
Largest diff. peak/hole / e Å^{-3}	0.56/-0.36	0.35/-0.33	0.57/-0.43

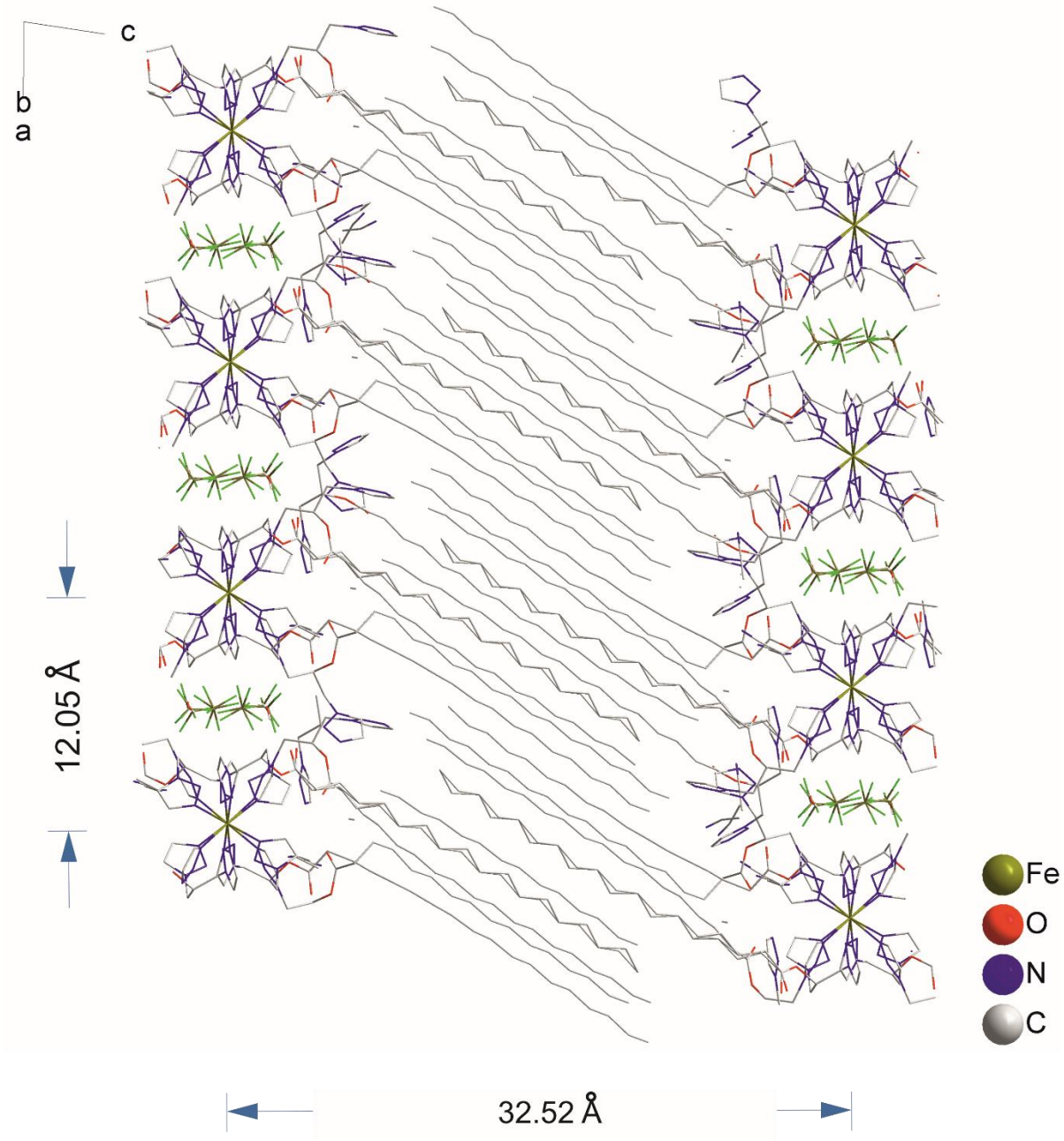

Figure S2. Thick lipophilic layer separates polar layers built from polymeric chains separated through counterions (250 K). Hydrogen atoms were omitted for clarity.

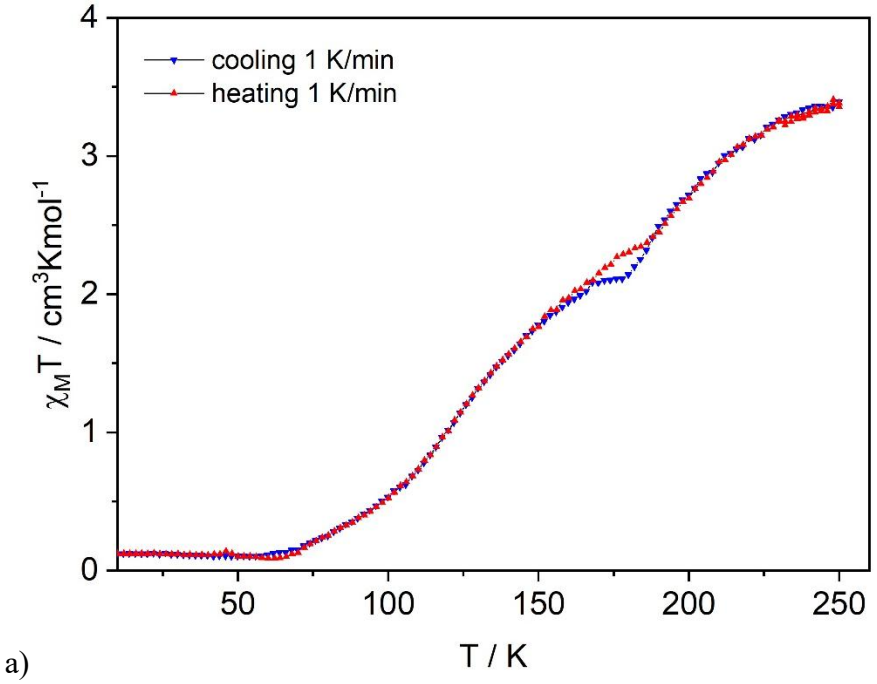

a)

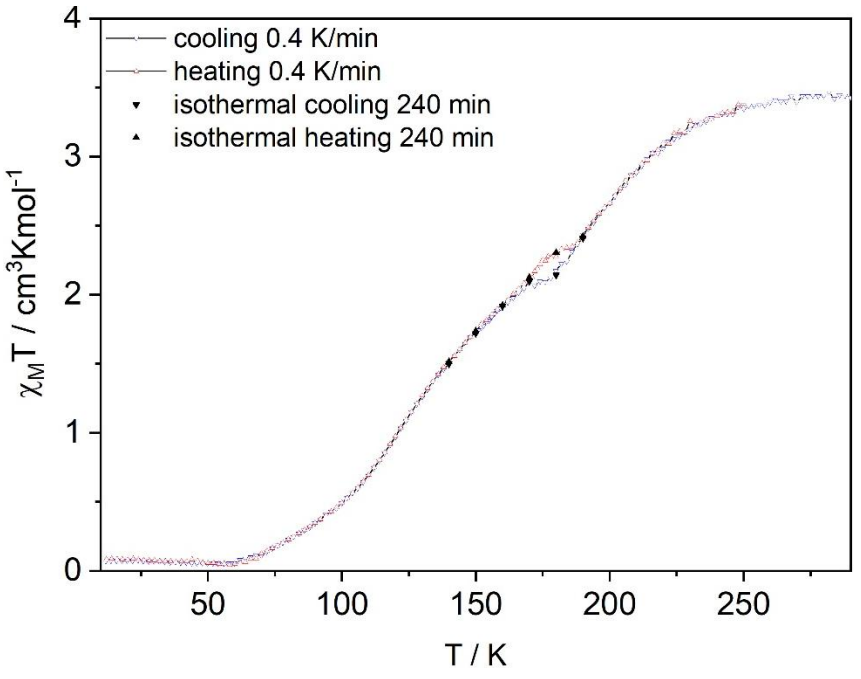

b)

Figure S3. $\chi_M T$ measurements performed on the second sample (crystalline) of **1**. Open symbols represent values recorded at a temperature scan rate of 0.4 K/min (a). During the measurement, the temperature change was stopped and an isothermal measurement was carried out. Black triangles represent $\chi_M T$ values recorded after 240 min. Measurement performed at a temperature scan rate 1 K/min is presented on (b).

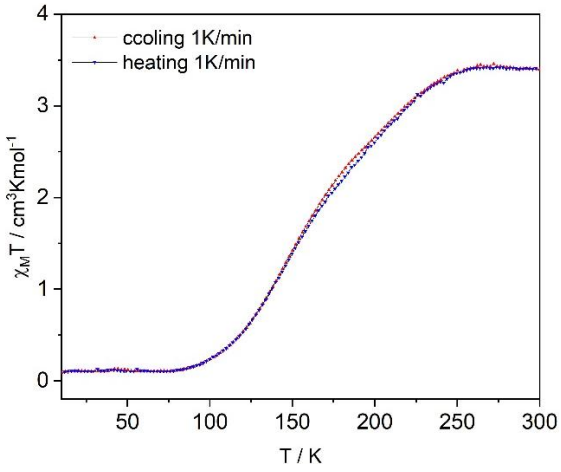

a)

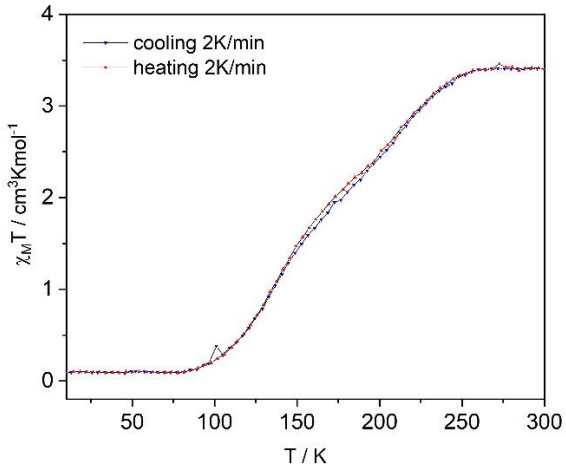

b)

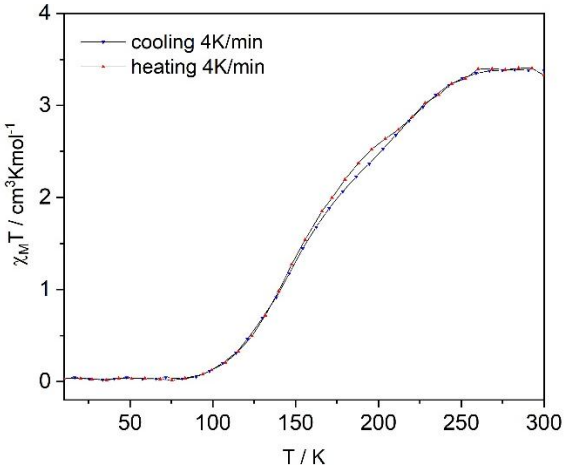

c)

Figure S4. $\chi_M T$ dependences (1, 2 and 4 K/min) obtained for third sample (crystalline) of **1**

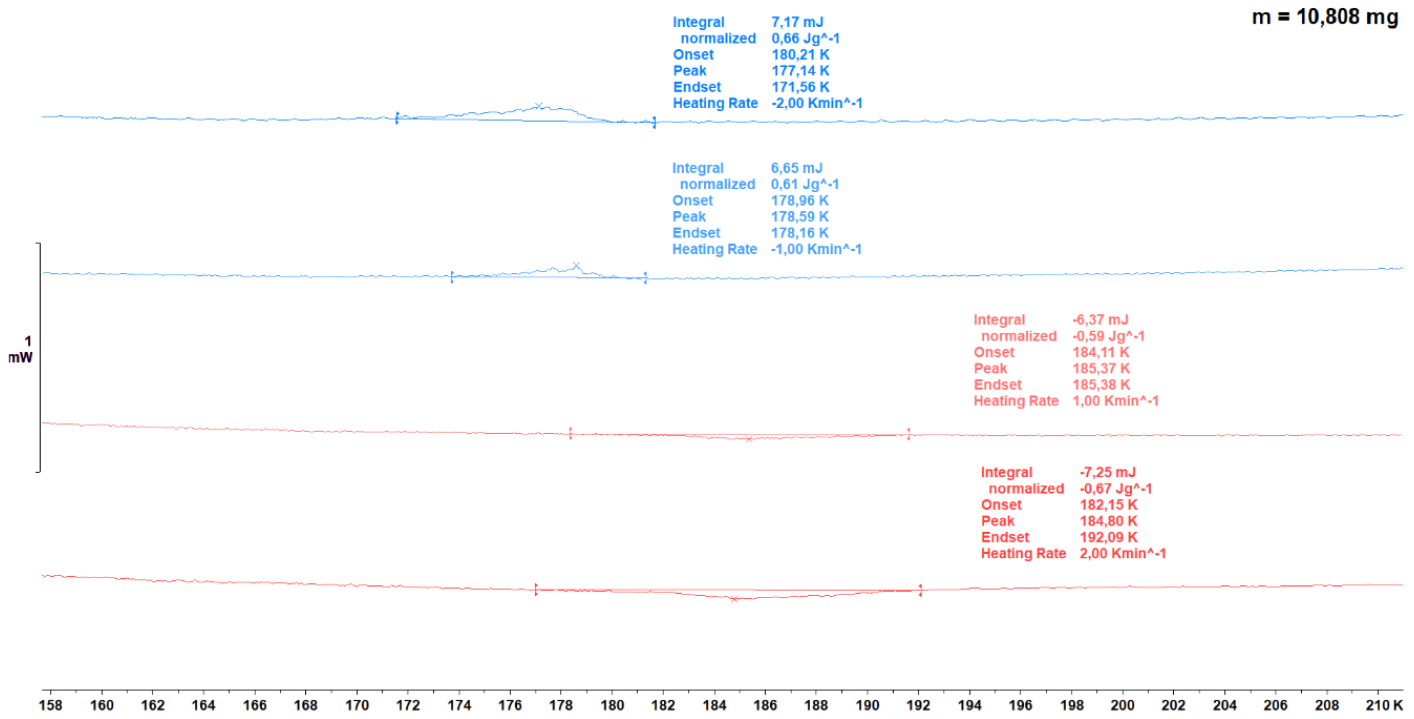

a)

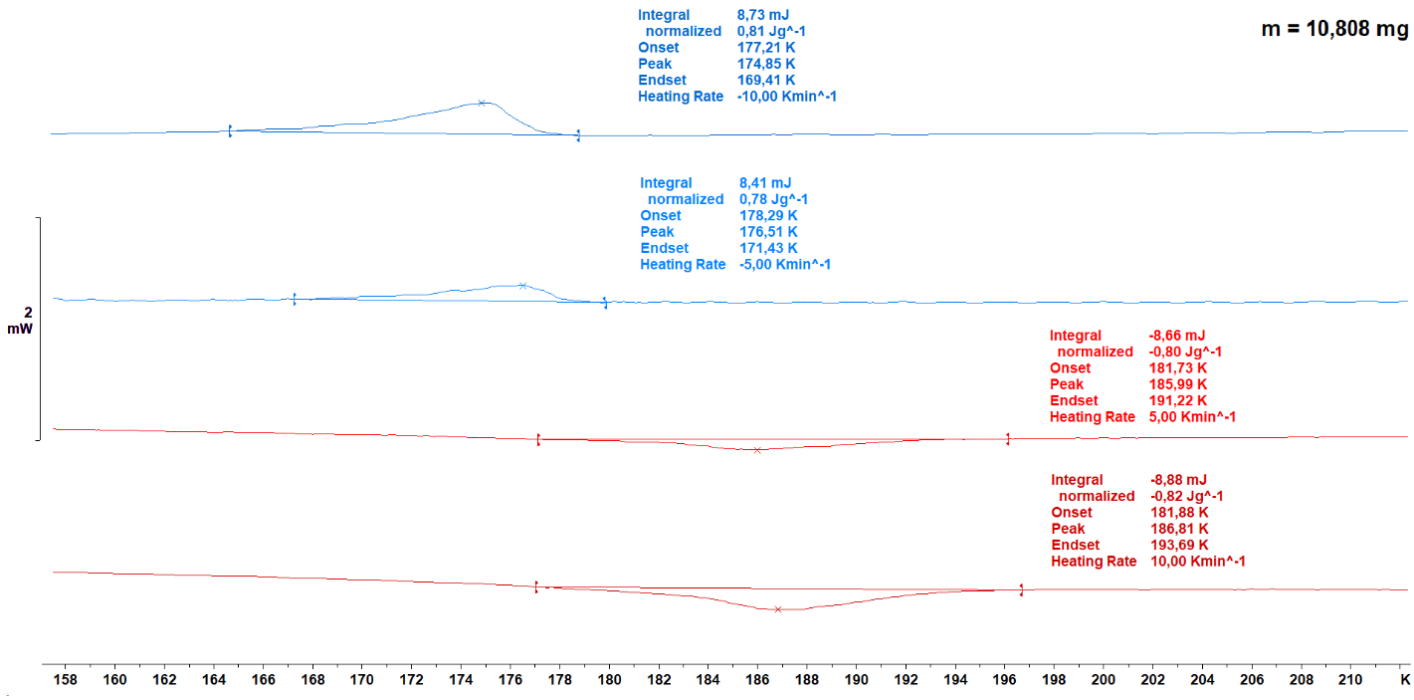

b)

Figure S5. DSC curve for **1** recoded at 1 and 2 K/min (**a**) and 5 and 10 (**b**) K/min in cooling (blue) and heating (red) mode.

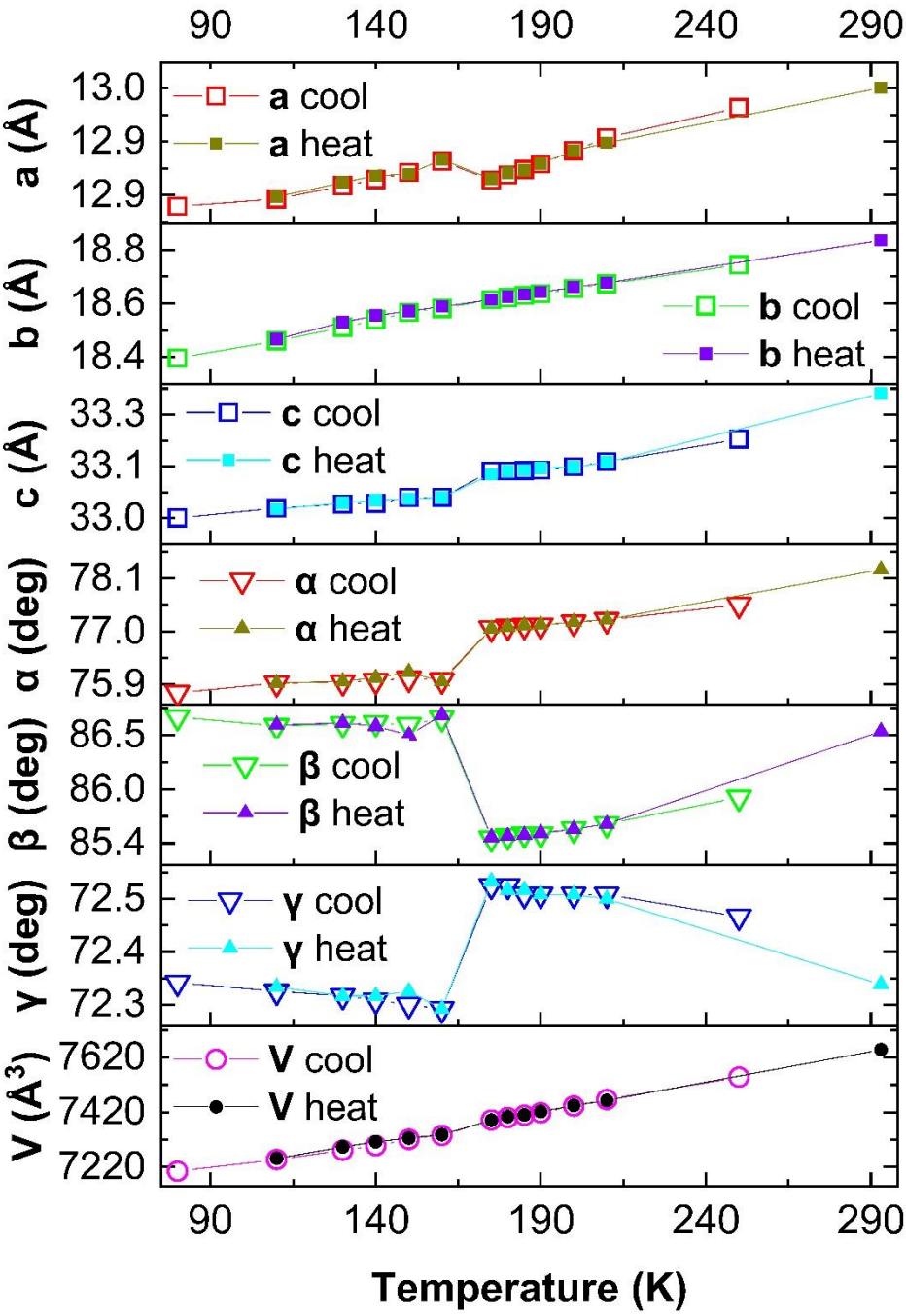

Figure S6. Temperature dependence of lattice parameters for **1**.

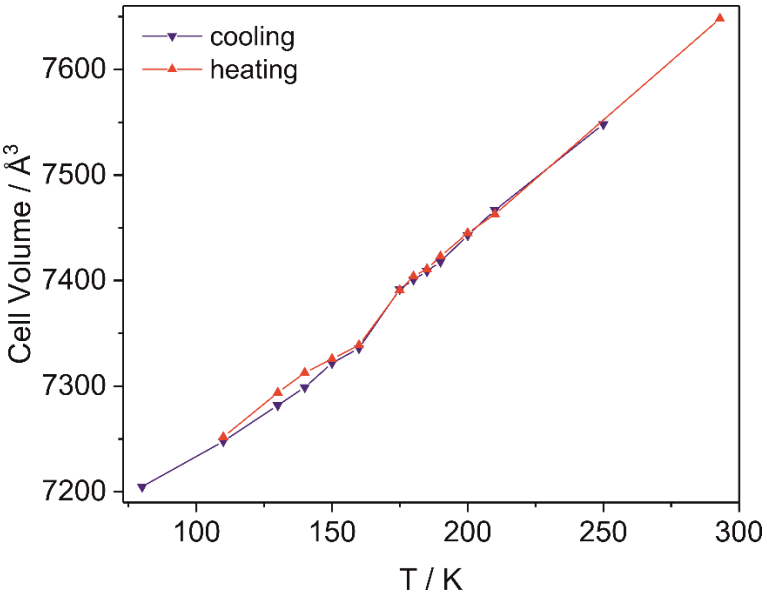

Figure S7. Temperature dependence of unit cell volume for **1**.

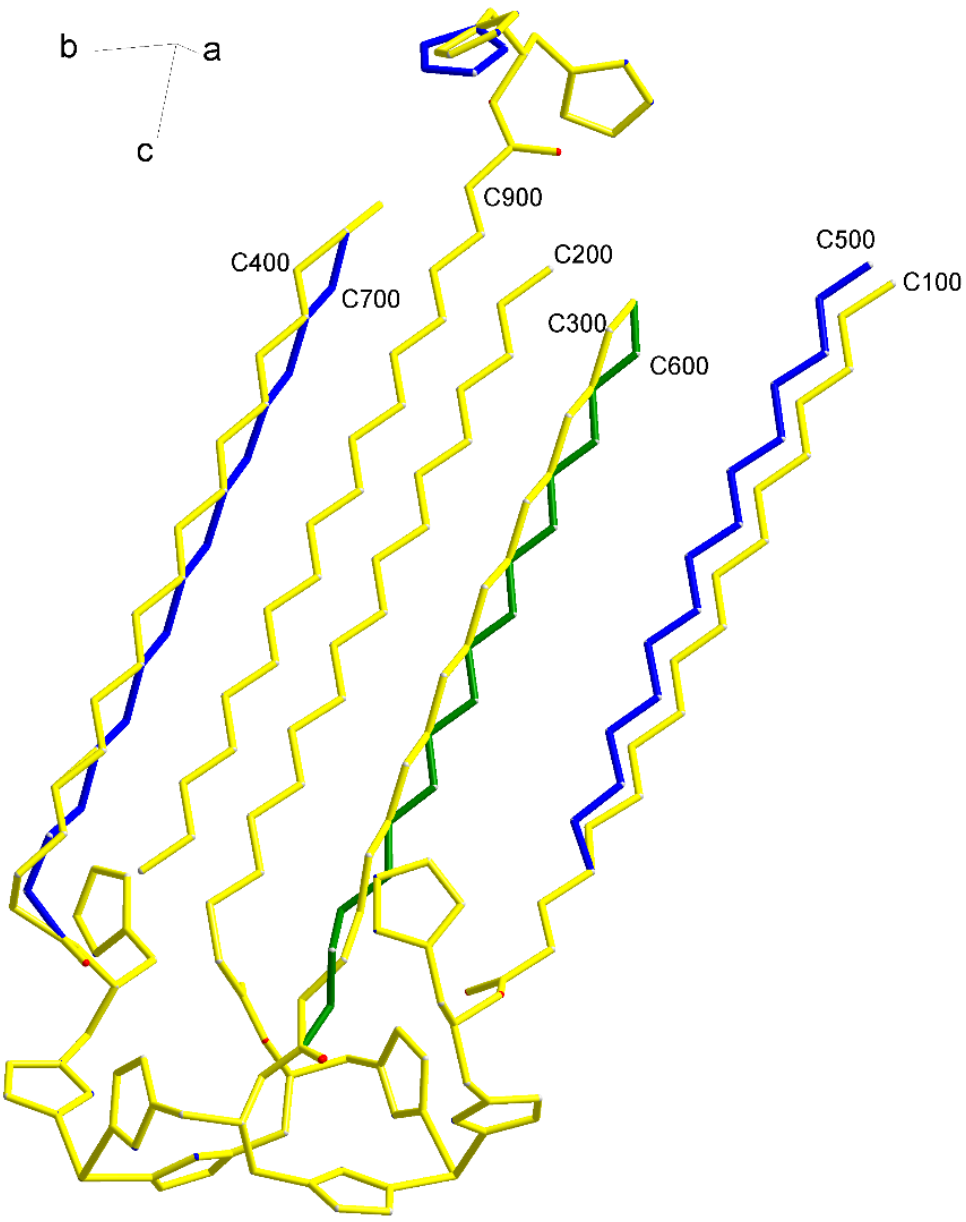

Figure S8. Yellow and green colors indicate conformers (independent part) present in the HS form (250 K) of **1**, while blue is used for conformers absent in the HS form. Hydrogen atoms, anions, acetonitrile and water molecules were omitted for clarity.

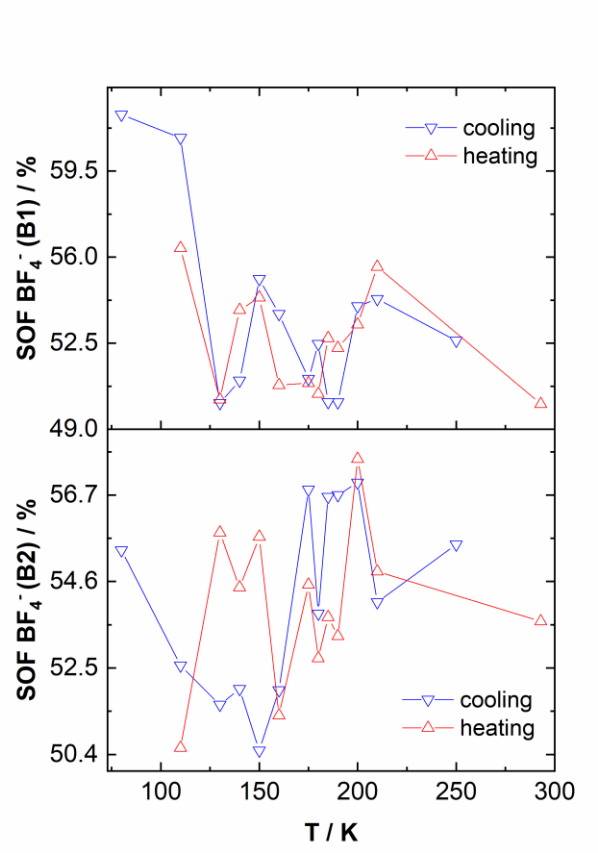

Figure S9. Temperature dependence of site occupancy factors for two crystallographically independent BF_4^- anions (site 1 and 2) in **1**.

Figures S6 and S7 show changes in lattice parameters, including the temperature dependence of the unit cell volume, and reveal subtle anomalies that can be assigned to a “reverse” spin transition. These changes are subtle, implying that only a small fraction of SCO centers are likely capable of switching their spin state in the reverse mode. It should be noted that the picture may be complicated by the formation of locally ordered structures or by domain formation. In such a scenario, the resulting “reverse” hysteresis would be broad but very shallow. In compound **1**, aside from the central region of the curve, the remainder clearly follows a typical “normal” spin crossover profile. We therefore propose tentatively that the observed “inverted” hysteresis arises from the superposition of two relatively independent but simultaneous occurred transformations:

(i) a thermally induced “normal” spin crossover driven by temperature change and lattice compression/expansion, and

(ii) a “reverse” spin transition triggered by structural rearrangements of the alkyl chains, which can locally perturb the Fe(II) coordination environment.

Under this scheme, the “normal” spin crossover behavior becomes modified, yielding lower $\chi_M T$ values upon cooling than upon heating. A schematic diagram illustrating the superposition of both transition types is provided below.

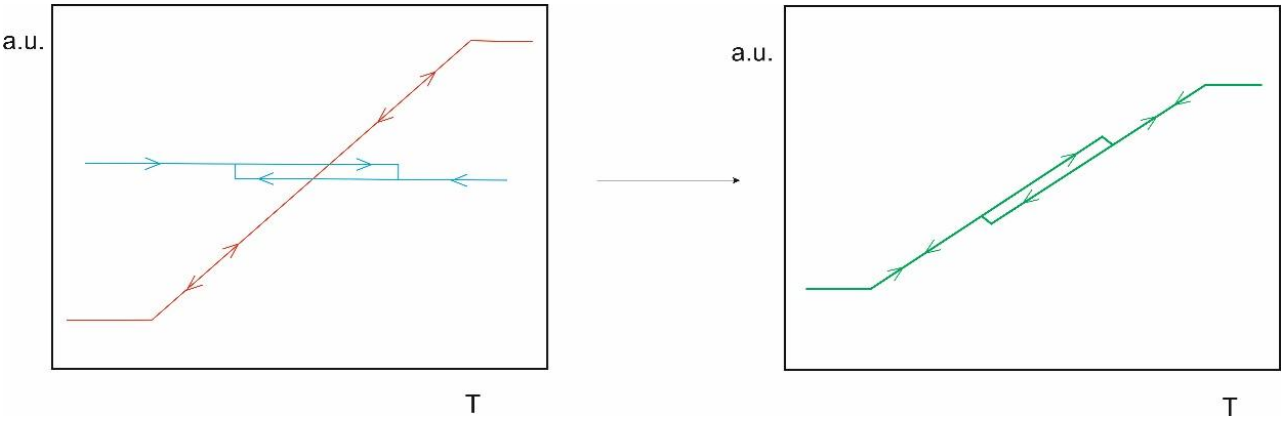

Figure S10. Graphical presentation of formation of “inverted” hysteresis in **1**.

Comments concerning crystal structures of 1.

The crystal lattice of complex **1** contains two bridging ligand molecules (C300/C600 and C200), two monodentately coordinated ligand molecules (C100 and C400), and one ligand molecule (C900) that acts as a guest species.

*Structure of ligand molecules in **1***. The conformations of the bis(1,2,3-triazol-1-yl)propylene fragments in the two bridging molecules are similar to each other. The differences between the corresponding torsional angles are less than 10°. One of the two bridging molecules is disordered, with the alternative positions of its alkyl chains (denoted C300 and C600) exhibiting a site occupancy ratio of 0.58:0.42. At 250 K, the planes of hydrocarbon chains C300 and C600 are tilted at an angle of approximately 60°.

Two main conformational types of the alkyl chains are present. The chains belonging to the disordered bridging ligand (C300/C600), one of the monodentate ligands (C100), and the uncoordinated guest molecule (C900) all adopt an extended zig-zag conformation. In contrast, the remaining two ligand molecules exhibit rotation around the C–C bond between the first two carbon atoms of the alkyl chain. For the second bridging molecule (C200), the corresponding torsion angle is 72°, while for the second monodentate ligand (C400), it is 67°.

A slight bending of the long alkyl chains in the bridging ligands is observed, which increases towards the polymeric skeleton (Fig. S8). The angle between the axis defined by the first three carbon atoms and the axis defined by the last three carbon atoms of the chain ranges from 2° to 11°. This bending is also present in the uncoordinated molecule.

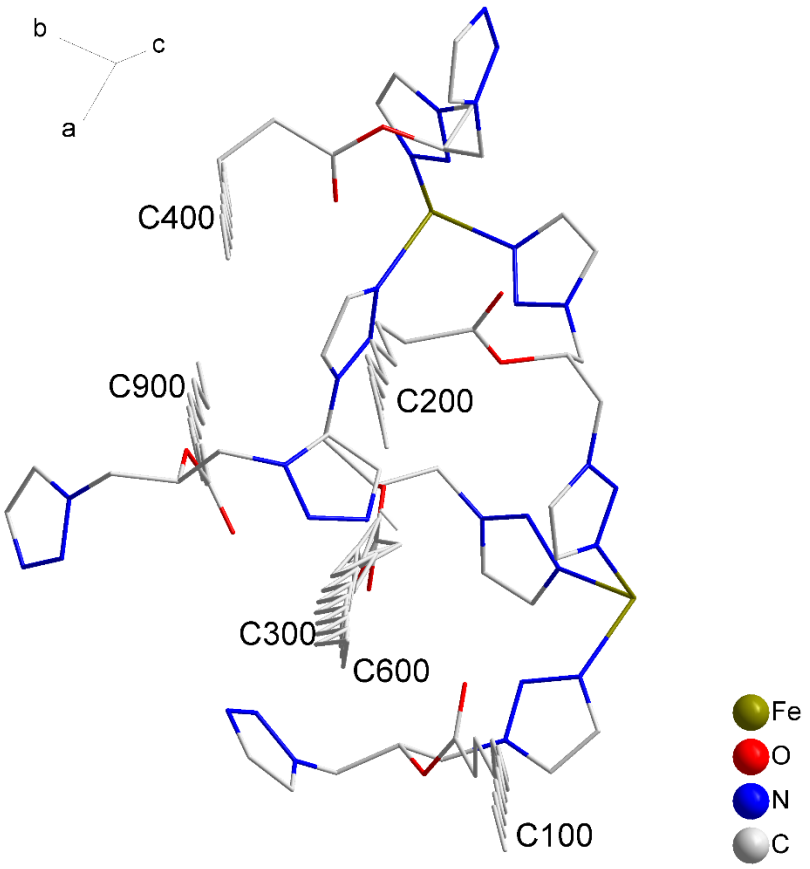

Figure S11. Picture showing bending of alkyl chains in **1** (250 K).

Bilayer arrangement. The bridging molecules C300/C600 and C200 connect Fe(II) ions along one direction, resulting in the formation of a one-dimensional polymeric chain. At 250 K, these chains assemble within the *ab* plane, separated by a distance of 12.0 Å, to form polar, macrocationic layers (Fig. S2). The distance between adjacent, parallel-oriented layers is 32.5 Å. Disordered tetrafluoroborate anions are located within the interlayer spaces, while disordered acetonitrile molecules occupy the peripheral regions of these spaces.

The alkyl chains of all **L1** molecules, including the non-coordinated ones, are oriented into the regions between neighboring macrocationic layers. This arrangement creates a thick, continuous lipophilic domain. The angle between the alkyl chains and the axis of the polymeric chain (defined by the bridged Fe(II) ions) is approximately 72°.

Conformational changes within spin crossover area. Cooling the crystal to 190 K does not induce structural changes beyond the slight shortening of the Fe–N bonds. Further cooling, however, leads to fundamental reorganization of the lipophilic part of the structure (Fig. 2, Fig. S6).

Below 190 K, new conformers appear for the C100 and C400 molecules, and the occupancy ratio of the C300/C600 conformers also changes. The most complex transformation occurs for the monodentate ligand C400. Its alkyl chain adopts a *syn* conformation in the vicinity of the bis(1,2,3-triazol-1-yl)propylene moiety. Upon cooling below 190 K, approximately 8% of these chains (assigned as a new site, C700) reorient. A plateau in this transition is observed between 175 K and 185 K. Further cooling then drives the rotation of ~45% of the C400 chains associated with moving away of resulting conformer C700 from the polar polymeric backbone. This results in an angle of 82° between the planes of the chain fragments in the extended conformation.

For the other monodentate ligand, C100 (which maintains a full *zig-zag* conformation), its chain splits into two distinct positions beyond the first three carbon atoms attached to the carbonyl group. As the temperature decreases, the occupancy of the new conformer (C500) gradually increases. Below 175 K, this increase becomes abrupt, leading to a C100:C500 occupancy ratio of 0.57:0.43 at 160 K. The planes of two alternative chains are parallel to each other.

The disordered bridging molecule C300/C600 also undergoes minor conformational changes, but the shift in site occupancies is less pronounced. The established disorder pattern is preserved, with only slight adjustments: the tilt angle changes to ~74°, and the occupancy ratio refines to ~0.55:0.45. In contrast, the C200 bridging molecule shows no temperature-induced conformational change. No conformational changes are observed for the alkyl chain of the uncoordinated ligand molecule. Instead, disordering of one of its triazole rings emerges. Upon continued cooling to 80 K, the occupancy factors for the coordinated ligand molecules converge toward a ratio of approximately 1:1 (Fig. 4). During heating in the 130–160 K range, the site occupancies of the C700, C600, and C500 conformers are slightly higher than those observed during cooling. Upon heating above 175 K, the behavior diverges for each ligand system. For the C400/C700 system, the return to the initial C400 conformer proceeds in two distinct steps, with the heating branch of the second step shifted to higher temperatures. In contrast, for the C300/C600 and C100/C500 systems, the heating branches lie clearly above the cooling branches up to approximately 190– 200 K.

Table S3. Geometric parameters of the weak interactions in the crystal structure of the ligand **L1** at 100 K. Distances are given in Å, angles – in degrees.

C-H···A	H···A	D···A	<(DHA)
C101-H10B···N132	2.59	3.173(4)	117.4
C123-H12A···N103[b]	2.74	3.478(4)	131.8
C123-H12B···O122[c]	2.57	3.506(3)	156.8
C34-H34···N133[d]	2.63	3.482(4)	148.8
C35-H35···N102[b]	2.72	3.527(4)	143.7
C35-H35···N103[b]	2.45	3.365(4)	162.6
C102-H102···N102[a]	2.61	3.517(3)	150.7
C105-H105···N102[a]	2.63	3.485(3)	150.0
C105-H105···N103[a]	2.30	3.243(3)	170.0

[a] -1+X,+Y,+Z; [b] -1+X,1+Y,+Z; [c] 1+X,+Y,+Z; [d] 1-X,1-Y,-Z

Table S4. Geometric parameters of the weak interactions in the crystal structure of the coordination compound **1** at 293 K, 250 K, 80 K. Distances are given in Å, angles – in degrees.

Temperature	**80 K**			**250 K**			**293 K**		
Spin state	**LS**			**HS**			**HS**		
C-H···A	**H···A**	**D···A**	**<(DHA)**	**H···A**	**D···A**	**<(DHA)**	**H···A**	**D···A**	**<(DHA)**
C101-H10A···F15[c]	2.22	3.098(7)	146.4						
C101-H10A···F10[c]	2.55	3.29(1)	131.6						
C101-H10B···F11	2.40	3.11(1)	128.1	2.38	3.154(7)	135.7	2.39	3.163(7)	136.2
C101-H10B···O1[k]	2.54	3.49(2)	160.3						
C103-H10C···O222[k]	2.42	3.268(3)	143.8						
C103-H10D···N912[d]	2.53	3.497(4)	166.1						
C123-H12B···O922[d]	2.43	3.409(4)	169.4						
C203-H20C···F14[j]	2.59	3.11(1)	112.6						
C201-H20A···F14[j]	2.42	3.118(9)	127.0						
C201-H20A···F11[j]	2.57	3.24(2)	124.5						
C201-H20A···F16[h]	2.37	3.214(7)	143.0	2.46	3.307(8)	144.6	2.51	3.358(9)	145.3
C201-H20A···F12[h]	2.32	3.19(2)	146.3	2.23	3.034(9)	139.0	2.24	3.031(8)	138.5
C201-H20B···N912[e]	2.68	3.441(4)	134.0						
C223-H22B···O422	2.69	3.420(4)	130.4						
C324-H32D···O122	2.35	3.26(1)	152.0	2.47	3.42(2)	163.9	2.49	3.40(1)	155.7
C303-H30C···F8l	2.43	3.05(2)	120.5						
C303-H30D···N432[k]	2.42	3.307(4)	148.2						
C401-H40A···F4b	2.49	3.236(9)	131.9						
C401-H40A···F8b	2.55	3.22(1)	124.9						
C401-H40A···N432	2.64	3.175(4)	114.2	2.60	3.158(3)	116.2	2.62	3.164(4)	115.8
C403-H40C···O222	2.49	3.017(4)	112.8	2.62	3.111(3)	111.4	2.65	3.132(4)	111.0
C403-H40C···N132[j]	2.71	3.399(4)	126.9						
C403-H40D···O322[j]	2.62	3.387(3)	134.2						
C403-H40D···O1	2.47	3.42(1)	160.0	2.58	3.51(2)	160.1	2.64	3.57(4)	161.7
C903-H90C···F13[g]	2.39	3.22(1)	140.0						
C903-H90C···F15[g]	2.47	3.324(6)	144.0						
C903-H90C···F9[g]	2.34	3.15(2)	138.2						
C903-H90C···F10[g]	2.43	3.35(1)	155.0						
C903-H90D···F1[e]	2.56	3.45(2)	150.3						
C903-H90D···F3[e]	2.57	3.45(2)	146.8						
C903-H90D···F5[e]	2.52	3.45(2)	155.9						
C901-H90B···F13[g]	2.60	3.45(1)	144.1						
C114-H114···N312[h]	2.44	3.095(3)	125.9	2.61	3.281(3)	128.6	2.63	3.297(4)	129.0
C115-H115···N932[d]	2.35	3.204(5)	149.0						
C917-H917···O422[i]	2.67	3.581(6)	159.8						
C202-H202···F11[j]	2.54	3.09(2)	114.4						
C214-H214···O122	2.33	3.258(4)	163.9	2.49	3.422(3)	169.9	2.54	3.459(4)	170.7
C216-H216···F1[f]	2.46	3.34(2)	155.6						
C216-H216···N332[a]	2.73	3.367(3)	125.0						
C217-H217···F13j	2.38	3.33(1)	172.8						
C217-H217···F14[j]	2.54	3.229(8)	129.9						

C217-H217···F9[j]	2.40	3.34(2)	171.0						
C217-H217···F11[j]	2.56	3.29(2)	133.6						
C314-H314···F13				2.54	3.02(1)	111.8	2.54	3.02(1)	112.6
C314-H314···F16	2.42	3.222(8)	142.6	2.47	3.294(8)	146.7	2.49	3.301(9)	146.4
C314-H314···F12	2.57	3.39(2)	144.6	2.50	3.37(1)	155.3	2.54	3.41(1)	155.9
C314-H314···N212[h]	2.60	3.265(3)	127.7						
C315-H315···F13	2.39	2.95(1)	117.3	2.46	2.97(1)	114.2	2.48	2.98(1)	113.8
C315-H315···F9	2.36	2.93(2)	118.3	2.40	2.981(9)	119.6	2.43	3.010(8)	120.4
C315-H315···F2[h]	2.43	3.20(1)	138.4	2.60	3.35(1)	136.4	2.66	3.39(1)	136.7
C315-H315···F3[h]	2.55	3.21(1)	127.0	2.66	3.27(1)	123.3	2.65	3.28(1	125.2
C315-H315···F6[h]	2.40	3.20(2)	141.2	2.38	3.199(9)	145.1	2.40	3.219(9)	147.0
C315-H315···F7[h]	2.50	3.078(9)	119.4	2.66	3.16(1)	113.9	2.67	3.17(1)	114.6
C402-H402···O222	2.68	3.310(3)	121.3						
C414-H414···N40[b]	2.70	3.21(2)	114.3						
C414-H414···N933[i]	2.70	3.341(5)	125.0						
C414-H414···N232[a]	2.73	3.330(3)	121.4						
C415-H415···F4b	2.62	3.07(1)	109.2						
C415-H415···N40[b]	2.64	3.18(1)	115.9						
C415-H415···C61[b]	3.01	3.82(2)	143.9						
C92-H92O···F4				2.24	3.19(2)	165.7			
C92-H92O···F3							2.56	3.40(2)	146.1
C92-H92P···N50				2.58	3.39(2)	141.1			

[a] 1-X,1-Y,2-Z; [b] -1+X,1+Y,+Z; [c] 3-X,-Y,2-Z; [d] 2-X,-Y,1-Z; [e] 1-X,-Y,1-Z; [f] 1-X,-Y,2-Z; [g] -1+X,+Y,-1+Z; [h] 2-X,-Y,2-Z; [i] 1-X,1-Y,1-Z; [j] -1+X,+Y,+Z; [k] 1+X,+Y,+Z; [l] +X,1+Y,+Z

References

1 G. M. Sheldrick, SHELXT - Integrated space-group and crystal structure determination. *Acta Crystallogr., Sect. A:Found. Adv.* 2015, **71**, 3– 8, DOI: 10.1107/s2053273314026370

2 G. M. Sheldrick, Crystal Structure Refinement with SHELXL. *Acta Crystallogr., Sect. C: Struct. Chem.* 2015, **71**, 3– 8, DOI: 10.1107/S2053229614024218

3 O. V. Dolomanov, L. J. Bourhis, R. J. Gildea, J. A. K. Howard, H. Puschmann, OLEX2: a complete structure solution, refinement and analysis program. *J. Appl. Crystallogr.* 2009, **42**, 339–341, DOI: 10.1107/S0021889808042726

4 H. Putz, K. Brandenburg, *Diamond - Crystal and Molecular Structure Visualization*; Crystal Impact GbR, 2014

5 A.L. Spek, *J. Appl. Cryst*. 2003, **36**, 7-11. Single-crystal structure validation with the program PLATON.